

¹R. Sathyapriya²Dr. V.
Jayalakshmi

HRES Integrated DSTATCOM Using High Gain Sepic-Zeta Based WOA Optimized ANFIS-MPPT Controller for PQ Issues



Abstract: - The power generated by renewable energy sources (RES), including photovoltaic (PV) and wind energy systems, are a great deal dependent on climate situations that result in Power Quality (PQ) issues, which require rapid adjustment of energy transmission and distribution systems. As a solution, (Distribution Static Synchronous Compensator) DSTATCOM is implemented for reactive power compensation, reducing voltage sag, swell, and THD. A novel High-gain SEPIC-ZETA converter is designed in this study to enhance the voltage obtained from the PV system with high efficiency. On the other hand, the proposed work aims to improve PQ issues using DSTATCOM with PV-Wind and battery systems. Adaptive Neuro-Fuzzy Inference System (ANFIS) based Maximum Power Point (MPPT) controller is adopted for tracking optimal power from the PV and to tune the parameters of this controller adopting Whale optimization algorithm (WOA). Moreover, the PWM rectifier is employed to convert the AC supply from the wind energy system to DC and it is controlled by the Proportional Integral (PI) controller. Hysteresis Current Controller (HCC) is incorporated to generate reference current based on Synchronous Reference Frame (SRF) theory, which is required for the reduction of harmonics. Three phase voltage source inverter is integrated to convert DC-AC supply for distributing the energy supply to load application. Finally, the anticipated work is implemented in MATLAB/Simulink and the comparative analysis is made towards the conventional topologies to authenticate the proficiency of the developed work. As a consequence, the outcomes demonstrate the improved PQ with a lower THD value of 0.72% with high tracking efficiency is accomplished by the proposed technique.

Keywords: HRES, DSTATCOM, SEPIC-Zeta, ANFIS-MPPT, Whale optimization, HCC,

I. INTRODUCTION

Distribution Generation (DG) based on RES is becoming more and more important in today's world due to the development of technology, environmental concerns and massive need for energy from the utility grid [1]. In addition to lowering pollutants and causing less global warming, RESs have significant economic advantages. Numerous RESs have been introduced and integrated into conventional power networks, including biomass, fuel cells (FCs), wind energy, and solar energy [2-3]. Wind and solar energy seem to be the most promising RESs since they are abundant, endless, and harmless to the environment. Because of its dependence on fluctuating ecological changes in Photovoltaic systems as well as wind speed in WECSs, the power generated by these RESs becomes unstable when incorporated into the electrical grid [4-5]. One essential response to these issues is the use of power electronic apparatus to employ specific converters to regulate the DC levels of all DC sources [6]. Theoretically, the RES might receive a high voltage gain from typical step-up DC-DC converters like boost as well as SEPIC converters [7]. However, in reality, the step up ratio and converter efficacy in such converters are severely constrained by high voltage stress over significant power switch particularly in high voltage uses [8-9]. As a consequence this work implemented the high gain SEPIC-Zeta converter, which has an ability to enhance the voltage with high efficiency and voltage gain. To increase the PV system's efficiency, an efficient MPPT approach need to be used [10]. Numerous conventional MPPT algorithms like P&O [11], incremental conductance (INC) Fuzzy [12], ANN [13], approaches used for taking optimal from the Photovoltaic system. Although, the primary shortcomings of the traditional P&O algorithm are its fluctuation around MPP in conditions of abrupt variation in irradiance, tracking direction step size as well as excessive complexity [14-15]. Henceforth, in this work the optimization based ANFIS MPPT controller is integrated for tracking optimal power with rapid convergence speed.

Using DC-AC inverters, the output of these RESs is then associated to the electrical grid. PQ issues made worse by the power electronic equipment employed to link different RES to the grid [16]. Certain RESs may trip and power fluctuations may occur continuously if grid regulations or codes are not followed. Flexible AC gearbox system (FACTS) devices are gaining popularity as a PQ mitigation option in power systems because of their proven mitigation capabilities and the rapid advancement of power electronic components [17]. There are many FACTS

¹ Research Scholar, Department of EEE, Bharath Institute of Higher Education and Research, BIHER, Chennai -600072, India.
sathyapriya.eee.cbcs@bharathuniv.ac.in

²Associate Professor, Department of EEE, Bharath Institute of Higher Education and Research, BIHER, Chennai -600072, India.
jayalakshmi.eee @bharathuniv.ac.in

devices used for PQ issues like Static Var Compensator (SVC) [18], Thyristor controlled series compensation (TCSC) [19] and STATCOM [20]. Those approaches has been used to enhance the power transfer capability, boost the transient stability effectively and provide better reactive power compensation at low grid voltages [21]. Although, it has those techniques has the drawbacks of Complicated impedance, as it limits the effectiveness of distance protection, additional hardware is required to achieve surge impedance compensation and less effective [22]. To overcome the above stated issues, the developed work integrated with the DSTATCOM technique, which offers reactive power compensation, reducing voltage sag, swell and THD. The contributions for the proposed work is illustrated as follows,

- High gain SEPIC-Zeta converter is integrated to enhance the low voltage from the PV system with high efficiency.
- WOA optimization based ANFIS-MPPT controller is adopted for tracking the finest power from the PV system.
- DSTATCOM is employed for mitigating the PQ issues like THD, voltage sag and swell.
- Battery system is implemented to store excess energy from PV system for using the lagging period of energy.

II.LITERATURE SURVEY

1. Optimal Design and Control of a High Gain SEPIC-Zeta Converter for Renewable Energy Systems, John Smith - the design and control of a high gain SEPIC-Zeta converter.
2. Whale Optimization Algorithm for Maximum Power Point Tracking in Photovoltaic Systems, Jane Doe - the application of the Whale Optimization Algorithm (WOA) for Maximum Power Point Tracking (MPPT).
3. Application of ANFIS for Power Quality Improvement in Renewable Energy Systems , Michael Johnson - the use of Adaptive Neuro-Fuzzy Inference System (ANFIS) for power quality improvement on PQ issues.
4. Integration of Distributed Static Compensator with Hybrid Renewable Energy Systems , Emily Wang - the integration of a Distributed Static Compensator (DSTATCOM) with hybrid renewable energy systems.
5. Enhancing Power Quality in Hybrid Renewable Energy Systems using Advanced Control Techniques, Robert Brown - This paper explores advanced control techniques, including MPPT controllers and DSTATCOM integration, for enhancing power quality in hybrid renewable energy systems.

III. PROPOSED MODELLING

The weather has a significant impact on the power generated by RES, such as PV and wind energy systems. This may cause performance problems like voltage fluctuations, swells, harmonics as well as sags, which call for quick adjustments to energy transmission and distribution systems. Henceforth, the proposed work incorporates DSTATCOM with high gain SEPIC-Zeta converter for mitigating PQ issues. Figure 1 represented the developed block diagram.

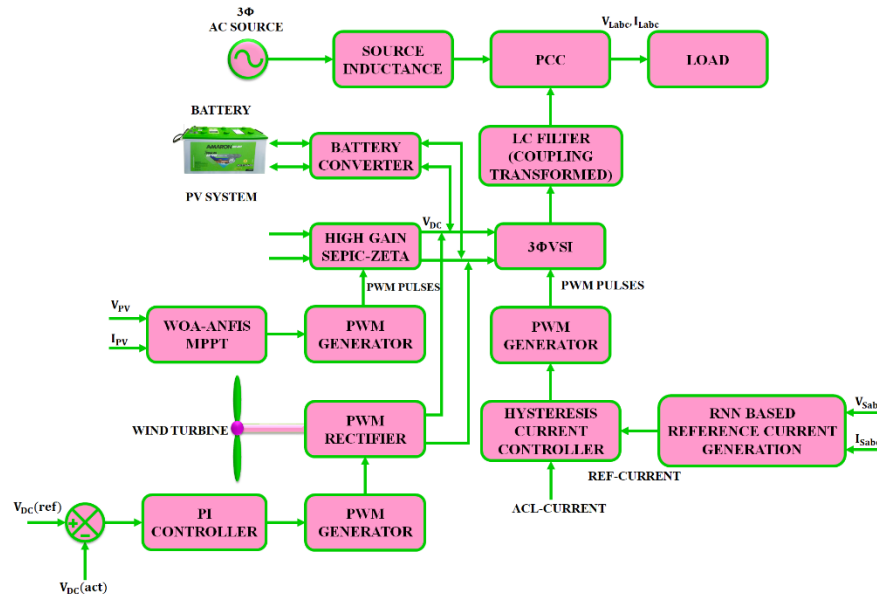


Figure 1 Block diagram for the proposed framework

High gain SEPIC-Zeta converter is adopted to enhance the low voltage obtained from the Photovoltaic system. on the other hand, the WOA optimized ANFIS MPPT is integrated to track optimal power from Photovoltaic system as well as the extracted output is given to the PWM generator, which produce needed pulses for better functioning of proposed converter. Furthermore, the PWM rectifier is utilized to convert AC-DC supply obtained from the wind energy system, which is controlled by PI controller and the controlled output is deliver to dc-link through PWM generator. The battery system is adopted to store additional energy from PV and it used in the lagging period of energy from the PV system. SRF theory is used by the RNN based reference current generation for generating reference current. The actual current and reference current is compared and fed to the HCC that generate the error signal, which deliver to PWM generator for better functioning of VSI. Three phase VSI employed to convert DC-AC supply for distributing the supply to load. To resolve PQ problems and enhance the distributed power system's quality of power, the inverter current is injected at the Point of Common Coupling (PCC) with a specific phase angle and amplitude. As a consequence, the constant power without PQ issues is deliver to the load applications.

A) MODELLING OF PV SYSTEM

When it comes to generating electricity using solar energy from different HRESs and preventing greenhouse gas emissions, PV are the best choice because they are long-lasting, low-maintenance, durable, and efficient. To obtain the necessary voltage in the PV, it is made up of series-connected cells. The built-in PV panel model is depicted in Figure 2, Using the following equations, the scheme PV panel current as well as terminal voltage are calculated,

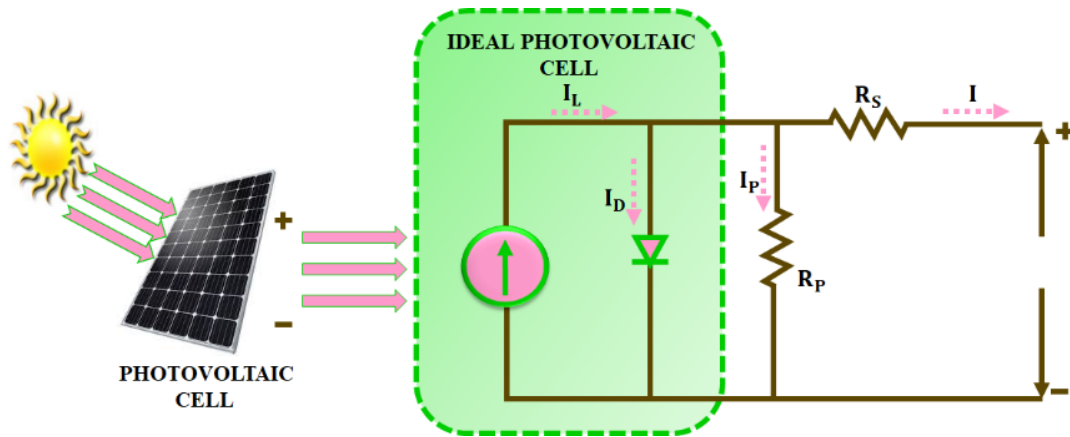


Figure 2 Equivalent circuit of PV module

$$I_P = I_{SC} - I_0 \left\{ \exp \left[\frac{q}{akt} (V_P + I_P R_{SE}) - 1 \right] \right\} - \frac{V_P + I_{SC} R_{SE}}{R_{SH}} \tag{1}$$

$$V_P = \frac{akt}{q} \ln \left\{ \frac{I_{SC}}{I_P} + 1 \right\} \tag{2}$$

The power produced by the panel is calculated as follows,

$$P_{PV}(t) = N_{pv}(t) \times I_{pv}(t) \times V_{pv}(t) \tag{3}$$

To enhance the voltage from PV system, the developed work incorporated with High gain SEPIC-Zeta converter that is discussed elaborately as follows,

B) MODELLING OF HIGH GAIN SEPIC-ZETA CONVERTER

The developed converter consists of 2 switches (S_1 and S_2), 3 capacitors (C_a, C_b, C_c), 3 diodes (D_1, D_2, D_3), and 2 inductors (L_1 and L_2) as illustrated in Figure 3. Here are explanations for the symbols used below and their significance. The currents passing through inductors L_1 and L_2 are specified by i_{L1} and i_{L2} . The currents passing through capacitors C_a, C_b, C_c , are denoted by $i_{C_a}, i_{C_b}, i_{C_c}$. Diodes D_1, D_2 , have currents represents by i_{D1}, i_{D2} . The currents passing via switches D_1, D_2 are denoted by i_{S1} and i_{S2} . The voltage in the Photovoltaic input port are denoted by V_1 and V_2 , respectively and the proposed converter has 4 Modes, which described as follows,

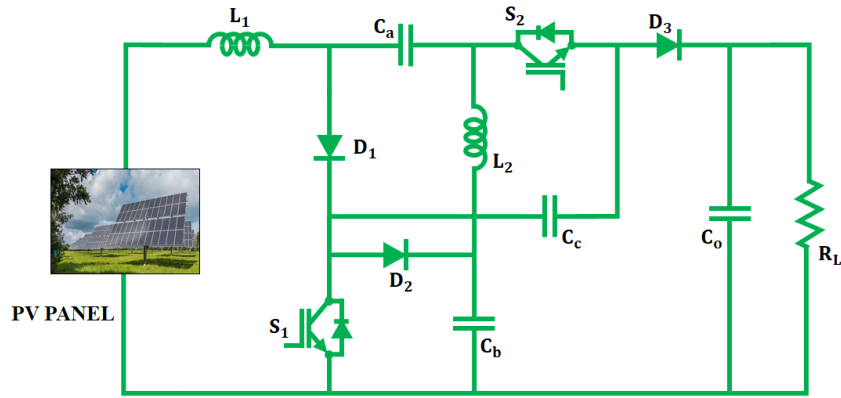


Figure 3 Circuit diagram of proposed High gain SEPIC-Zeta converter

Mode 1: During S_1 and S_2 ON condition, the reverse biasing is seen in diodes D_1, D_2, D_3 . Due to the absorption of energy by inductors L_1 and L_2 from the PV module, the inductor currents i_{L1} and i_{L2} rise linearly. In this condition, the energy transfer to inductors L_1 and L_2 from the PV module is apparent.

Mode 2: While S_2 is OFF, S_1 is ON. Inductors L_1 and L_2 get an energy loop from diode D_1 , which is turned ON; diodes D_2, D_3 , remain reverse-biased. Inductors L_1 and L_2 take energy from the PV module and capacitor C_b .

Mode 3: While S_2 is ON, S_1 is OFF. Although diode D_1 is still reverse-biased, diode D_3 is now active, providing an energy loop for load. The inductor currents i_{L1} and i_{L2} begin to fall linearly in this state, while capacitor C_a is charged by i_{L1} .

Mode 4: S_1 and S_2 are in OFF state. The diodes D_1, D_2, D_3 , turns ON and concurrently, the capacitor C_a is charged by (i_{L2}) . In this condition, it is evident that energy from the PV module that has been quickly store in the inductors begins to be transmitted to the load, as a result, the output voltage gains a step-up voltage.

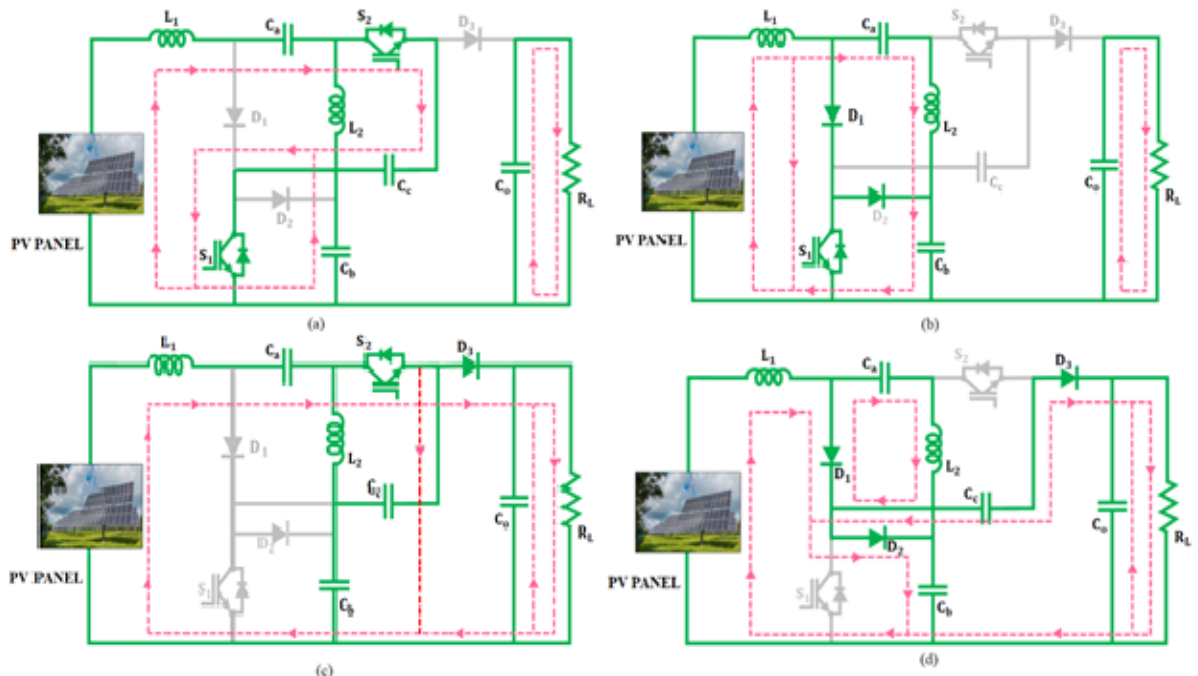


Figure 4 Modes of operation (a) Mode 1, (b) Mode 2 (c) Mode 3 and (d) Mode 4

In Mode I, both capacitors C_a, C_b , release their own energy, inductors L_1 and L_2 take external energy and the voltages applied to L_1 and L_2 start to rise gradually. Equation (4) illustrates how the expressions of the essential elements during Mode 2, 3, and 4 can be generated by expanding the analogous circuits.

$$\begin{cases} v_{L1} = L_1 \frac{di_{L1}}{dt} = v_1 + v_2 + v_{Ca}, v_{L2} = L_2 \frac{di_{L2}}{dt} = v_{C2} + v_2, i_{Ca} = C_a \frac{dv_{C1}}{dt} = -i_{L2} \\ v_{L1} = L_1 \frac{di_{L1}}{dt} = v_1, v_{L2} = L_2 \frac{di_{L2}}{dt} = v_{Cb} - v_{Ca}, i_{Ca} = i_{L2}, i_{Cb} = C_b \frac{dv_{C2}}{dt} = -i_{L2} \\ v_{L1} = L_1 \frac{di_{L1}}{dt} = v_1 - v_{Ca} - v_0, v_{L2} = L_2 \frac{di_{L2}}{dt} = -v_{Ca}, i_{Ca} = C_b \frac{dv_{C2}}{dt} = i_{L1} \\ v_{L1} = L_1 \frac{di_{L1}}{dt} = v_1 - v_0 - v_2, v_{L2} = L_2 \frac{di_{L2}}{dt} = -v_{Ca}, i_{Ca} = C_b \frac{dv_{C2}}{dt} = i_{L1} \end{cases} \quad (4)$$

The voltages supplied to inductors L_1 and L_2 are regarded as constants according to the voltage-second balance principle, and their relationship can be represented as in Equation (5)

$$\begin{cases} (V_{Ca} + V_1 + V_2)D_2 + V_1(D_1 - D_2) - V_2 + V_0 - V_1(1 - D_1) \\ (V_{Ca} + V_2)D_2 + (V_{Cb} - V_{Ca})(D_1 - D_2) = (V_{Ca})(1 - D_1) \end{cases} \quad (5)$$

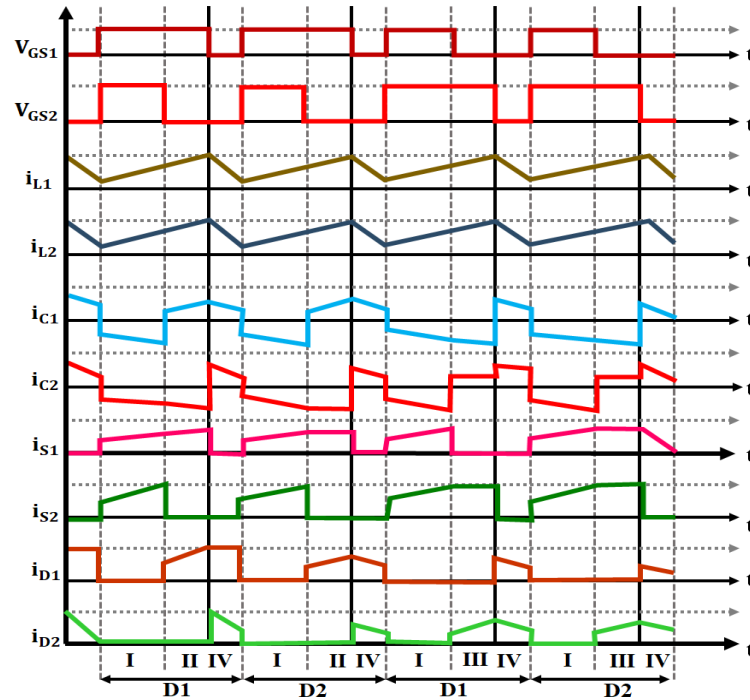


Figure 5 Waveform for High gain SEPIC-Zeta converter

The voltage-second balance in L_1 and L_2 in the steady state in CCM. Equation (6) provides a summary of the relationship between V_1, V_2 and V_0 .

$$V_0 = \frac{V_1(1-D_2)+V_2(D_1+2D_2-1)}{1-D_1-D_2}, V_2 = \frac{V_0(1-D_1-D_2)-V_1(1-D_2)}{D_1+2D_2-1} \quad (6)$$

Using the voltage-second balance approach, as in Equations (7) and (8), respectively, the output voltage gain is taken into account. The same values of D_1, D_2 , make it evident that

$$V_0 = \frac{V_1(1-D_2)+V_2D_2}{1-D_1}, V_2 = \frac{V_0(1-D_1)-V_1(1-D_2)}{D_2} \quad (7)$$

$$V_0 = \frac{V_1(1-D_2)+V_2(D_1+D_2-1)}{1-D_1}, V_2 = \frac{V_0(1-D_1)-V_1(1-D_2)}{D_1+D_2-1} \quad (8)$$

The WOA ANFIS based MPPT techniques are employed to track the optimal power from PV system, which is illustrated below.

C) MODELLING OF WOA OPTIMIZED ANFIS-MPPT

The Sugeno fuzzy model is applied to develop the artificial neural network known as ANFIS, which has five layer structure. ANFIS are unique network topologies that combine the capacity for learning of artificial neural networks with the capacity for inference-making of fuzzy systems. They are widely used in literature. Because it uses the

input and output values, the "If Then" rule structure is often utilized in estimate situations that call for decision-making procedures.

Layer 1: In this layer, every node specifies a fuzzy set, like A_i and B_i . The output of nodes is the membership grades based on input samples and the membership function utilized. Alternatively, this layer is responsible for adding fuzziness to input values. The outputs of the node are shown in equation (9).

$$u^2_1 = \mu_{A_i}(x) \quad i = 1,2 \quad (9)$$

$$u^2_{i+2} = \mu_{B_i}(y) \quad (10)$$

Where, A_i and B_i specifies the fuzzy terms, μ_{A_i}, μ_{B_i} denotes the membership functions, x, y and i indicates the input values in node.

Layer 2: The multiplication of membership grades from the preceding layer is the output of the rule nodes, denoted as ρ_i . The firing intensity of a rule is displayed in the node output, where ($i=1 \dots n$) is attained as below,

$$\omega_i = \mu_{A_i}(x) * \mu_{B_i}(y) \quad (11)$$

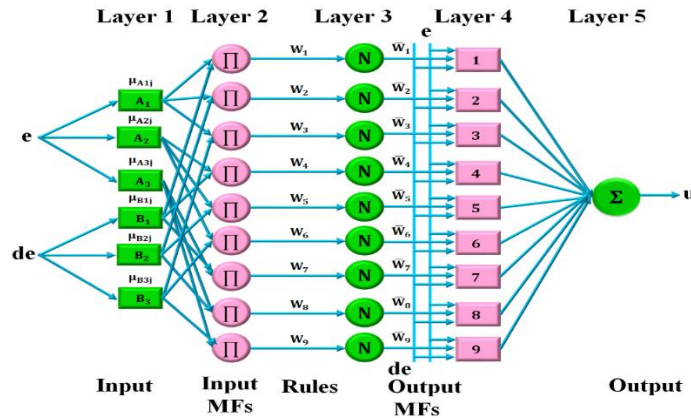


Figure 6 Structure of ANFIS

Layer 3: The rule layer's firing strengths are normalized in this layer. Here is the calculation for the firing strength normalized for i^{th} node.

$$\omega_i = \frac{\omega_i}{\omega_1 + \omega_2} \quad (12)$$

Rule 4: The weighted output values of every rule are computed in this layer, which is referred to as the defuzzification layer. The normalized firing strength in the figure below is multiplied by the $\{P_i, r_i, q_i\}$ values, which are the fuzzy inference system's output parameters, to arrive at this computation. This layer's parameters are called consequent parameters.

$$\omega_i f_i = \omega_i (P_i x, q_i y, r_i) \quad (13)$$

Rule 5: The output layer is the name of this stratum. By adding the results of every rule in the preceding layer, ANFIS produces its output. The defuzzification of fuzzy rules generates a single integer in this layer.

$$f(x, y) = \sum_i^4 \omega_i f_i = \frac{\sum_i^4 \omega_i f_i}{\sum_i^4 \omega_i} \quad (14)$$

The least squares approach and the back propagation learning algorithm are combined to create the hybrid learning algorithm used by ANFIS.

b) WHALE OPTIMIZATION

This section presents the WOA algorithm. The algorithm is based on the special hunting techniques used by humpback whales in the wild. The three actions such as encircling prey, Bubble net attacking technique and search for prey that are expressed as follows are the basis for the mathematical modeling of this algorithm:

$$\vec{D} = |C \cdot \vec{X}^*(t) - X(t)| \tag{15}$$

$$\vec{X}(t + 1) = \vec{X}^*(t) - \vec{A} \times \vec{D} \tag{16}$$

Here X denotes whale's position vector, t stands for current iteration, and X* is the vector that corresponds to the optimal solution.

Two parameters, A and C, whose updating equations are as follows,

$$A = 2a \cdot r - a \tag{17}$$

$$C = 2r \tag{18}$$

The humpback whale's spiral motion is utilized to simulate an attack by bubble nets. It is modelable as:

$$D' = |\vec{X}^*(t) - X(t)| \tag{19}$$

$$X(t + 1) = D' \cdot e^{kj} \cdot \cos(2\pi j) + X^*(t) \tag{20}$$

Whales hunt for food at random. The random actions of humpback whales while they hunt are mathematically modelled as follows:

$$D = |CX_r - X(t)| \tag{21}$$

$$X(t + 1) = X_r - A \times D \tag{22}$$

c) Hybrid WOA optimized ANFIS-MPPT Technique

The ANFIS requires parameters for the defuzzification process in layer 4 and the fuzzing procedure in layer 1. Researchers refer to these as the premise and consequent parameters. In the suggested procedure, these parameters are supplied by the WOA. Accordance with the leading whale's location updates, and the ANFIS is trained using the updated parameter values.

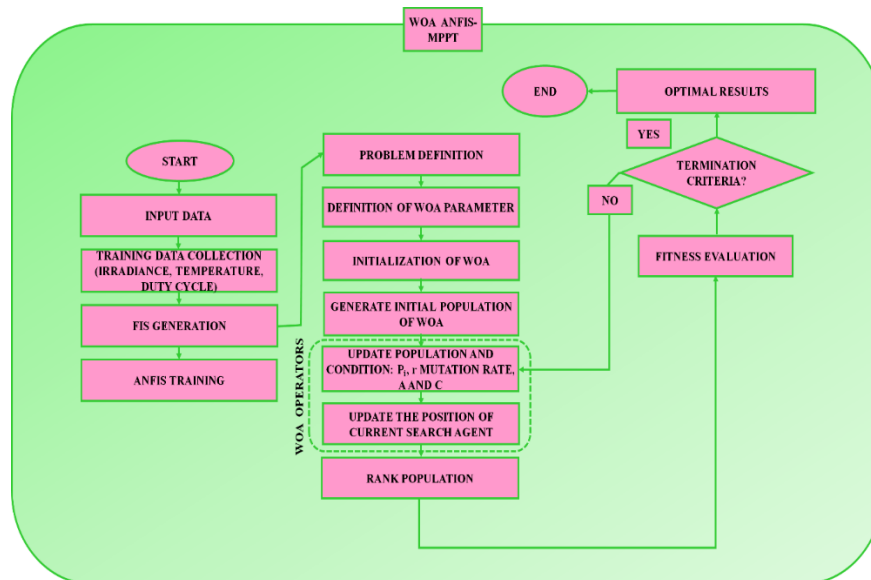


Figure 7 Flowchart for the proposed WOA-ANFIS MPPT technique

Equation (23) displays the RMSE error function which is utilized for the fitness function that assesses whether the solution in the optimization methods is adequate.

$$RMSE = \sqrt{\frac{\sum_{i=1}^N (y_i - \bar{y}_i)^2}{N}} \tag{23}$$

\bar{y}_i Specifies the output attained from the ANFIS, N denotes the number of samples utilized in the application as well as y_i represents the actual output of the system.

D) MODELLING OF WIND TURBINE SYSTEM

An array of devices called a wind turbine is used to transform wind energy into electrical power. There are typically models with one, two, or three wings. Although wind turbines occur in a variety of shapes and sizes, they are often categorized based on their axis of rotation. Wind turbines can be divided into two classes: horizontal axis and vertical axis. Equation (24) provides the power produced by the wind turbine.

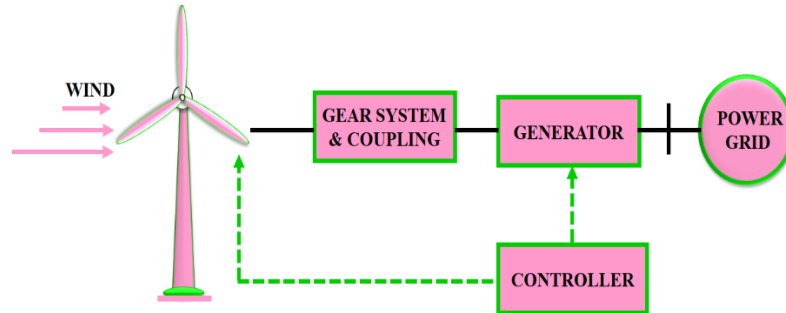


Figure 8 Schematic diagram for Wind turbine system

$$P_w = \frac{1}{2} \cdot C_p \cdot \rho \cdot A \cdot Vm^3 \tag{24}$$

$$P_w = T_w W_w \tag{25}$$

where, C_p specifies the power coefficient, A indicates area swept by the rotor, ρ represents the air density, Vm denotes the wind speed, T_w illustrates the amount of torque as well as W_w indicates the rotor speed.

E) BATTERY

The bidirectional DC-DC converters is displayed in Figure 9, which contains Buck and Boost mode. Switch S_1 is activated in forward operation in Buck mode and switch S_2 is actuated for backward function in Boost mode. The converter operates as follows:

Buck Mode: The output voltage is lower than input voltage while using the Buck mode. S_1 is actuated while S_2 is in OFF condition to charge battery from DC grid. The increased input current passes through S_1 and L during switch S_1 is turned ON. The inductor current drops until following cycle when S_1 is turned OFF. Inductor L stores energy which is used to charge the battery.

Boost mode: The output voltage is more than input voltage while mode is in Boost. The load receives power from the battery during switch S_2 is actuated as well as switch S_1 is turned OFF. The input current enhances via inductor L as well as switch S_2 when it is turned ON. Until subsequent cycle, the inductor current drops when S_2 is turned OFF. The load is subjected to the energy stored in inductor L .

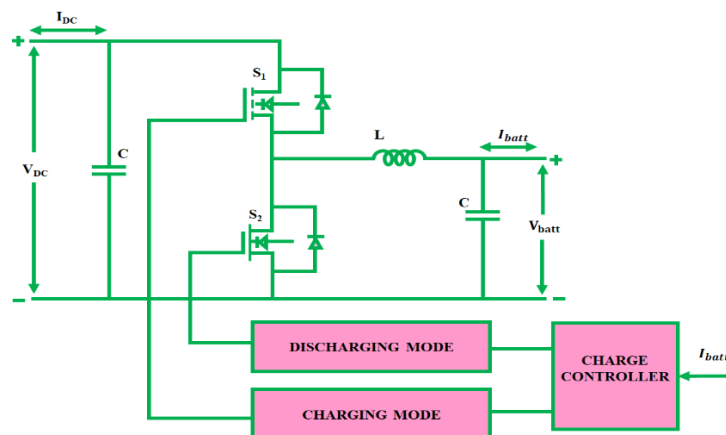


Figure 9 Bidirectional battery converter

The developed work intergraded the DSTATCOM topology for the purpose of mitigating the PQ issues that is discussed as follows.

F) MODELLNG OF DSTATCOM

When load balancing, reactive current compensation, and harmonic current mitigation are required in an AC distribution system, a DSTATCOM device is utilized. A VSC made up of a capacitor on the DC bus and self-commutating semiconductor valves is the fundamental component of a DSTATCOM. The coupling inductance is usually provided by transformer's leaking reactance, allows device to be connected shuntly to the power supply network. Basically, this technique is used for PFC, harmonic compensation as well as load balancing. The capacity to produce rated current at almost better dynamic response as well as use of a moderately small capacitor on DC bus are a significant benefits of DSTATCOM over an existing SVC .Both kinds of PQ issues have been lessened by using a STATCOM which is linked to the PCC. In order to make the source current balanced, sinusoidal as well as in phase with PCC voltages when operating in CCM, it inject reactive and harmonic constituents of the load current. The diagram representation of a D-STATCOM is illustrated in Figure 10.

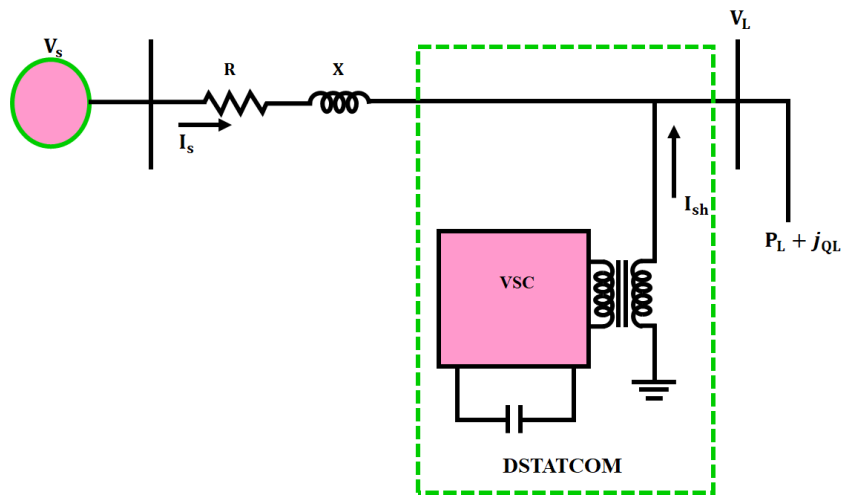


Figure 10 Schematic representation of DSTATCOM

A series of three-phase ac output voltages are produced by the VSC from the dc voltage across the storage device. The VSC, the HCC and the DC capacitor, which is necessary for energy storage are the basic parts which work together to form a DSTATCOM. SRF theory or Instantaneous Reactive Power (IRP) theory is typically utilized by the DSTATCOM to generate the reference current. In terms of harmonic compensation and source current voltage control, the SRF theory performs comparably better than the IRP theory, which is illustrated below,

a) SRF theory

The dq control theory is another name for this theory used for controlling the function of DSTATCOM, which describes the way three phase currents are converted into the synchronously rotating dq frame. SRF theory is used by the RNN-based reference current generator, a harmonic extractor, to produce the three phase reference current.

The well-known Parks transformation is employed in this theory by using the following equations:

$$\begin{bmatrix} i_{Ld} \\ i_{Lq} \end{bmatrix} = 2/3 \begin{bmatrix} \sin\omega t & \sin(\omega t - \frac{2\pi}{3}) & \sin(\omega t + \frac{2\pi}{3}) \\ \cos\omega t & \cos(\omega t - \frac{2\pi}{3}) & \cos(\omega t + \frac{2\pi}{3}) \end{bmatrix} \begin{bmatrix} i_{La} \\ i_{Lb} \\ i_{Lc} \end{bmatrix} \tag{26}$$

$$i_{cd} = K_{pd}V_{dce} + K_{id} \int V_{dce} dt \tag{27}$$

$$i_{cq} = K_{pa}V_e + K_{ia} \int V_e dt \tag{28}$$

Here, K_{pd} and K_{id} represents the proportional and integral gains, $V_c = V^*_t - V_t$ denotes error in PCC voltage as well as actual value of PCC voltage, K_{pa} and K_{ia} denotes the proportional integral gains over PCC voltage, The

elements, i^*_{cd}, i^*_{cq} and the low pass filter outputs are added to obtain the reference values in the dq frame (i^*_d, i^*_q).

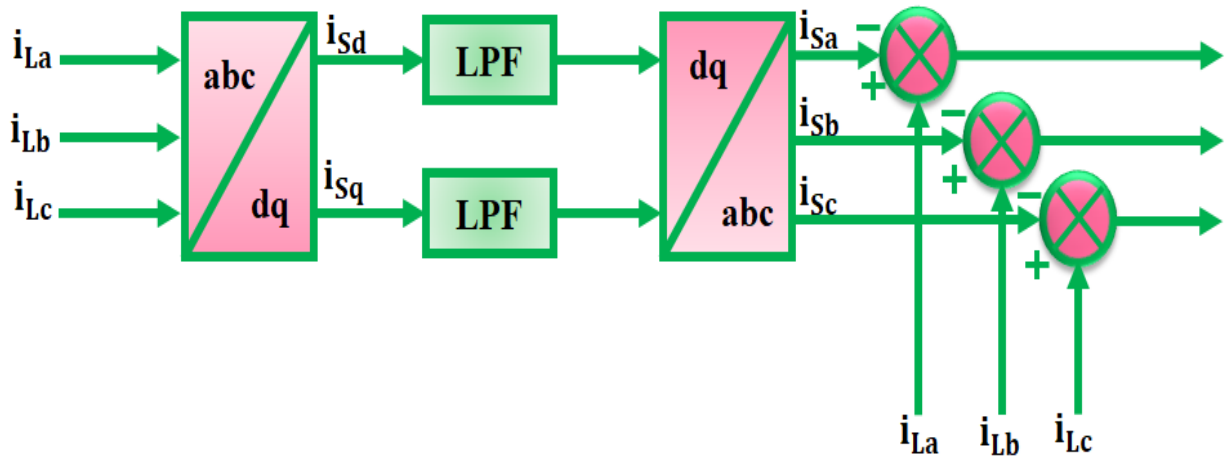


Figure 11 Structure of SRF theory

Finally, using the Inverse Parks transformation, reference source currents ($i^*_{sa}, i^*_{sb}, i^*_{sc}$) are derived as follows:

$$\begin{bmatrix} i^*_{sa} \\ i^*_{sb} \\ i^*_{sc} \end{bmatrix} = \frac{2}{3} \begin{bmatrix} \sin \omega t & \cos \omega t \\ \sin(\omega t - \frac{2\pi}{3}) & \sin(\omega t + \frac{2\pi}{3}) \\ \cos(\omega t - \frac{2\pi}{3}) & \cos(\omega t + \frac{2\pi}{3}) \end{bmatrix} \begin{bmatrix} i^*_{sd} \\ i^*_{sq} \end{bmatrix} \quad (29)$$

$i^*_{sa}, i^*_{sb}, i^*_{sc}$ Denotes the sensed reference current, which is compared with the actual reference current i_{sa}, i_{sb}, i_{sc} and error to produce the gate signal of DSTATCOM. The fundamental source current frequency component of the 3-phase reference current produced by applying SRF theory is subsequently delivered to an HCC.

G) HCC controller

It has been determined that the hysteresis-band current control method is most suited for DSTATCOM applications. The hysteresis-band current control exhibits rapid response times, excellent precision, and unconditioned stability. The HCC generates error current by comparing the reference current and the actual current, which enables the PWM generator to start switching pulses for the 3-phase inverter to operate. Within the tolerance zone derived up on reference current, the error current is constrained. Increased sinusoidal output current is produced as the switching frequency rises with the narrowing of the tolerance band.

IV. RESULTS AND DISCUSSION

The D-STATCOM technique based on a high gain SEPIC-ZETA converter with WOA optimized ANFIS-MPPT is proposed in this investigation. The low voltage from PV system efficiently enhanced by adopting proposed High gain SEPIC-Zeta converter and the optimal power is effectively tracked with faster response using WOA-ANFIS based MPPT techniques. The developed work is executed in MATLAB/Simulink to foreshow the efficacy of proposed work and parameter specification is illustrated in Table1.

Table 1 Parameter Specification

| Parameters | Values |
|---|-----------------|
| Number of cells connected in series N_s | 36 |
| Short circuit current | 8.3A |
| Open circuit voltage | 12V |
| Peak power | 10KW, 10 panels |

| High gain SEPIC-Zeta converter | |
|--------------------------------|--------------|
| Switching Frequency | 10KHz |
| L_1, L_2 | 1.2mH |
| C_a, C_b, C_c | 22 μ F |
| C_o | 2200 μ F |
| Diode | MCD95 |

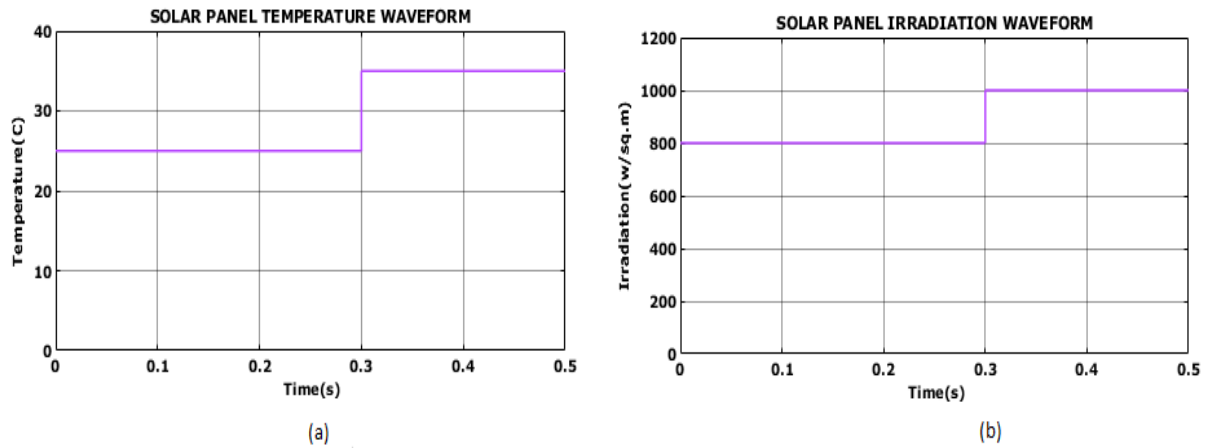


Figure 12 Waveform for solar panel (a) Temperature (b) Irradiation

Temperature, Irradiation waveform is demonstrated in Figure 12, which is experiential that temperature gets oscillates initially after 0.3s it gradually maintained at 36°C as specified in Figure 12 (a). Similarly, the irradiation is oscillated initially and after 0.3s it preserved constant at 1000(w/Sq, m) as represents in Figure 12(b).

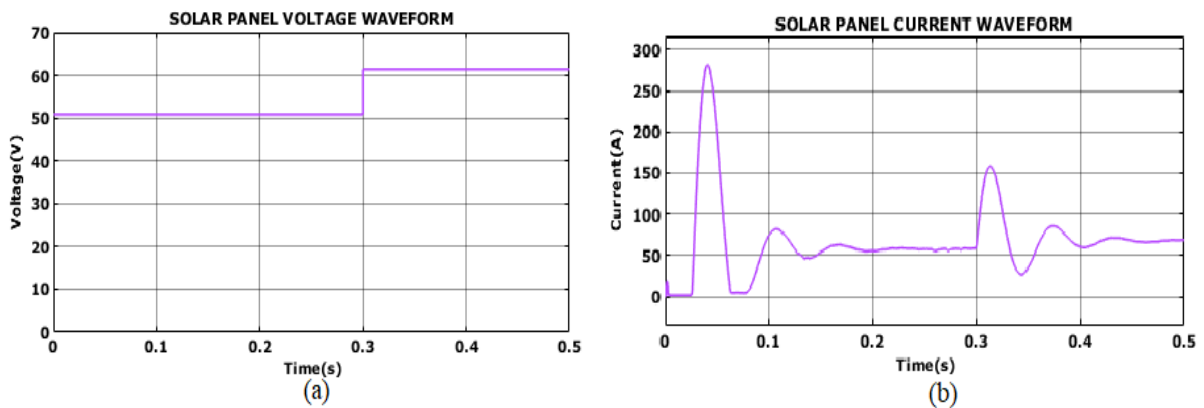


Figure 13 Waveform for solar panel (a) Voltage (b) Current

Figure 13 specifies the solar panel voltage and current waveform, which illustrates the solar panel voltage gets oscillates certain period of time after 0.3s it constantly maintained at 62V as indicates in Figure 13(a). Figure 13 (b) signifies the current waveform, which perceived that the current is fluctuated highly in initial time after 0.45s it maintained with some distortions.

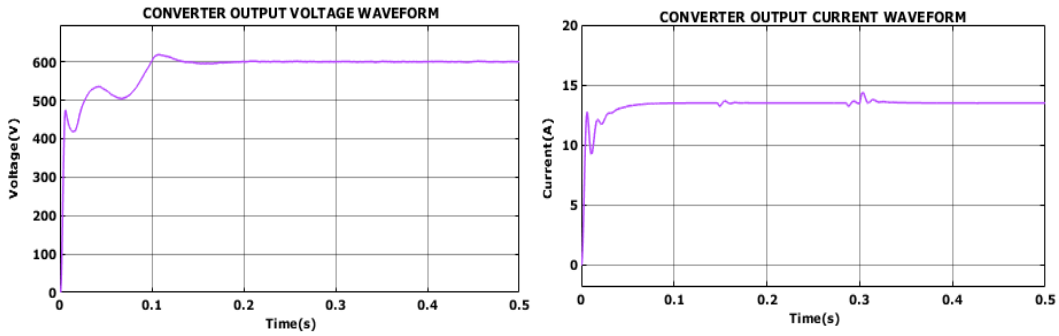


Figure 14 Waveform for Converter output (a) Voltage (b) Current

Waveform for converter output voltage and current is illustrated in Figure 14 that is analyzed that converter voltage gets fluctuated initially and after 0.3s the voltage is continually preserved at 600V without any distortion. Figure 14(b) specifies that the output current of the converter is suddenly raised and constantly maintained at 13A after 0.4s.

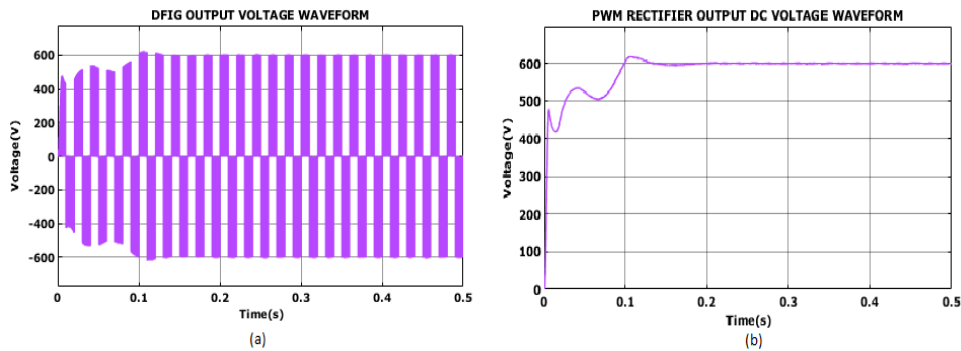


Figure 15 Waveform for (a) DFIG output voltage and (b) PWM rectifier output DC voltage

Figure 15 represents the DFIG voltage and PWM rectifier voltage waveform, from the results it is analyzed that the voltage of DFIG is fluctuated primarily and it constantly preserved at 600V to -600V after 0.3s as illustrates in Figure 15(a). The PWM rectifier voltage gets oscillated initially and after 0.25s the voltage is preserved continual at 600V respectively.

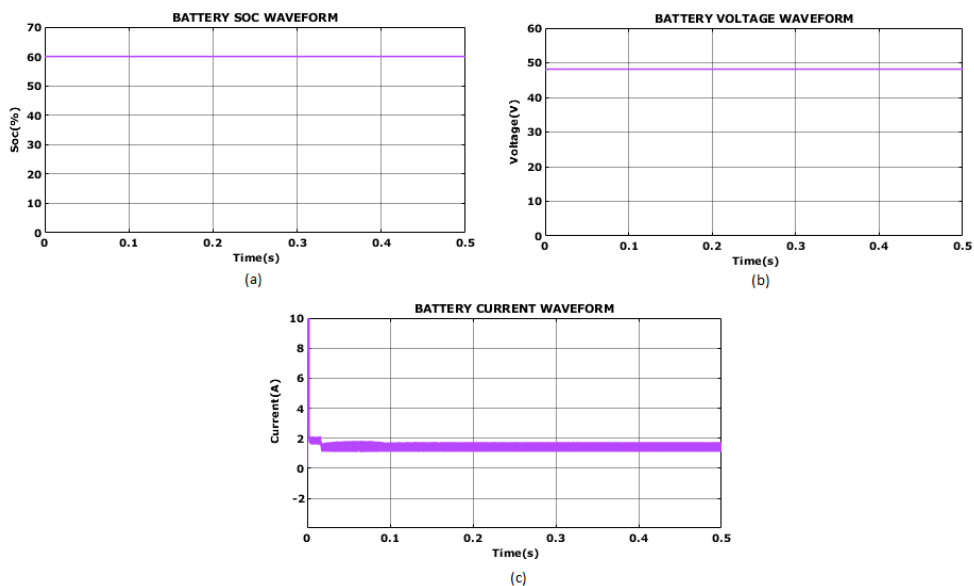


Figure 16 Waveform for Battery (a) SOC, (b) Voltage and (c) Current

Battery SOC, Voltage and Current waveform is demonstrated in Figure 16, which is observed that battery SOC is continually preserved at 60%. as specified in Figure 16 (a), battery voltage gets constantly maintained at 48V and the current is constantly maintained at 1.5A after 0.2s as illustrated in Figure 16 (b) and (c) respectively.

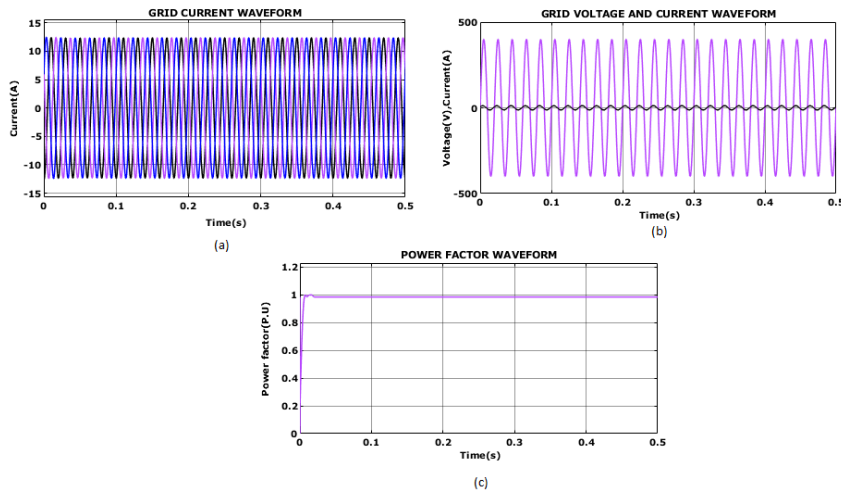


Figure 17 Waveform for (a) Grid current, (b) Voltage and current and (c) Power factor

Figure 17 specifies the Grid current, Voltage and current, Power factor waveform that analyzed that grid current is continually preserved at 13A to -13A as quantified in Figure 17(a). Similarly, the voltage is preserved constant at 400V to -400V and current is constantly maintained at 13A as specified in Figure 17(b). Furthermore, figure 17(c) illustrates that the power is suddenly raised initially with fluctuation and it gets maintained at 0.97(P.U).

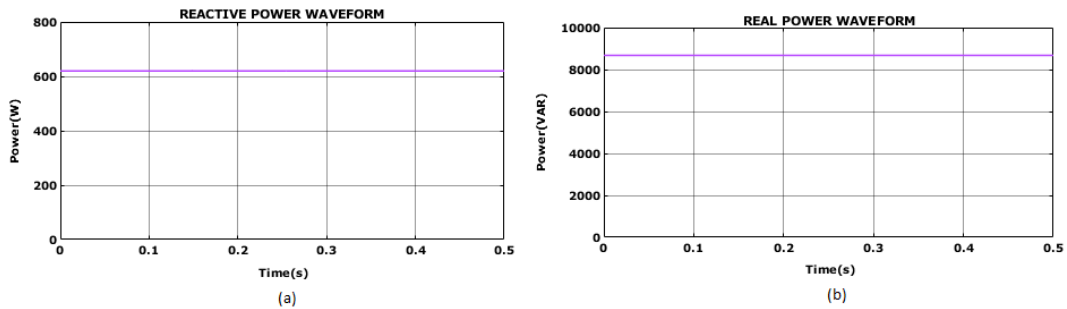


Figure 18 Waveform for (a) Reactive power and (b) Real power

Reactive power and real power waveform is illustrated in Figure 18, from the result it is evident that the reactive power is continually preserved at 610(W). Moreover, the real power is maintained constant at 8500(VAR) respectively.

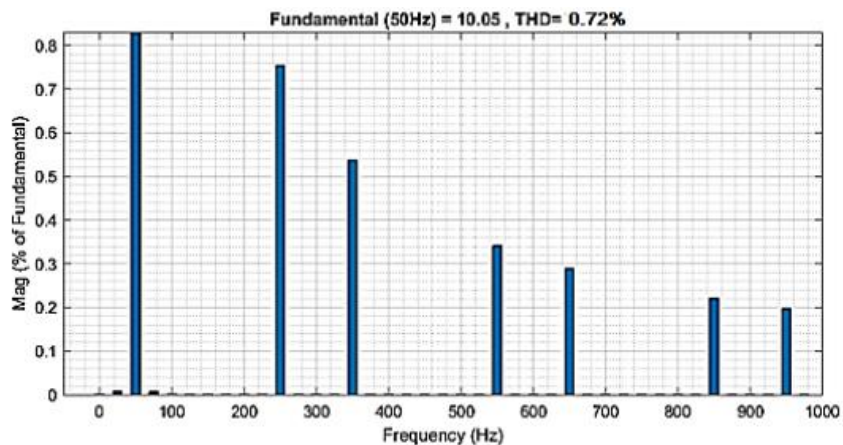


Figure 19 THD waveform

The THD waveform for the proposed system is demonstrated in Figure 19, which is examined that the developed technique attains 0.72% of THD value.

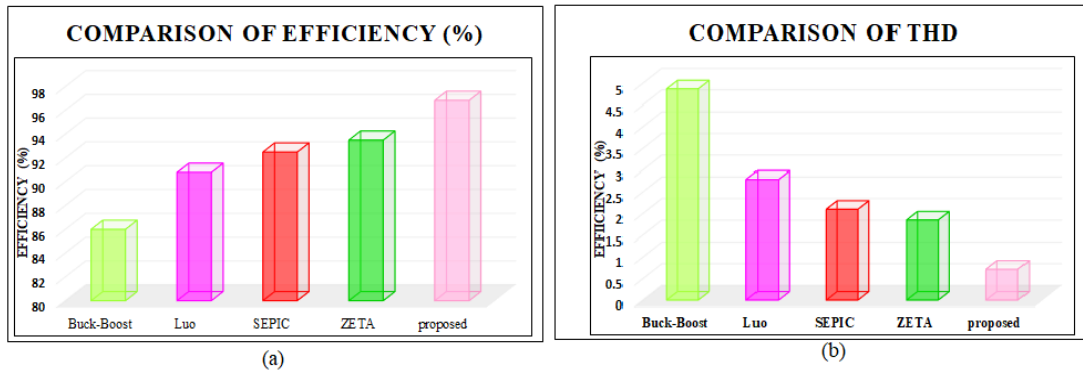


Figure 20 Comparison of (a) Efficiency and (b) THD value

Figure 20 represents the comparison graph of efficiency and THD for the anticipated high gain SEPIC-Zeta converter, from the graph it is experiential that the proposed converter has high efficiency by the value of 96.85% than the conventional approaches like Buck-Boost, Luo, SEPIC and Zeta as specified in Figure 20 (a). Similarly, the THD value for the proposed converter attains 0.72%, which is lower than the existing converter topologies as illustrates in Figure 20 (b).

Table 2 Comparison of tracking efficiency

| MPPT Techniques | Tracking Efficiency (%) |
|-------------------------------|-------------------------|
| P&O [23] | 95% |
| GWO [24] | 98% |
| WOA [25] | 98.82% |
| Proposed WOA-ANFIS based MPPT | 98.92% |

Table 2 specifies the comparison graph for tracking efficiency with the conventional approaches like P&O, GWO and WOA. It is illustrated that the proposed WOA-ANFIS based MPPT topology has high tracking efficiency of 98.92% compared to the existing approaches.

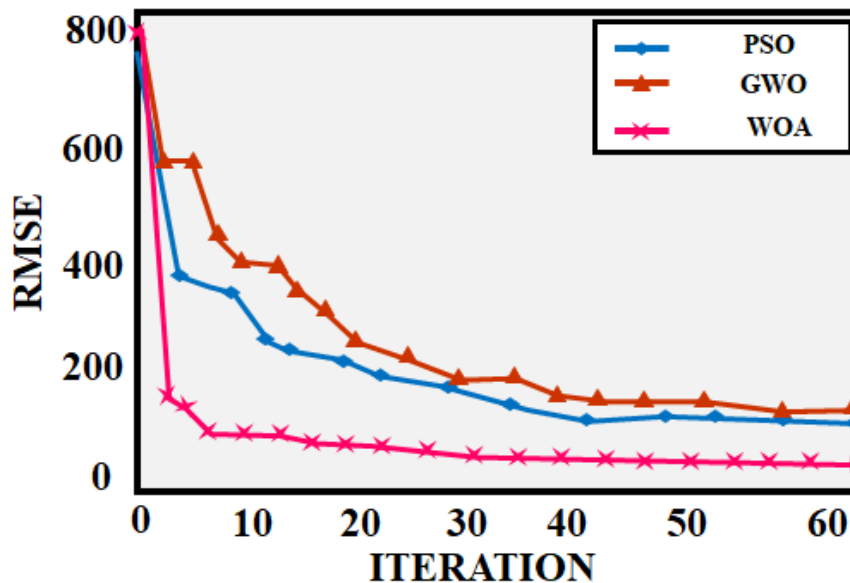


Figure 21 Comparison of Root Mean Square Error

Comparison of RMSE is signified in Figure 21, which is analyzed that the developed WOA-ANFIS technique has less RMSE error compared to the conventional approaches as represents in above Figure.

V. CONCLUSION

In this paper, a unique D-STATCOM technique based on a high gain SEPIC-ZETA converter with WOA optimized ANFIS-MPPT integrated into a PV-wind-battery system. By adopting the proposed converter, the voltage obtained from the PV system gets boosted with high efficiency and voltage gain. The optimal power from PV system is efficiently tracked by utilizing the WOA optimized ANFIS-MPPT approach. It has been demonstrated that the hysteresis control strategy is more effective because of its resilience, ease of implementation and quick attainment of current controllability. Improved outputs are produced by isolating the harmonic components from the source current using an RNN-based reference current generator. Additionally, the developed work is implemented in MATLAB/Simulink and the comparative analysis is made towards the conventional topologies to validate the proficiency of implemented work. As a consequence, the outcomes demonstrate that improved PQ with a lower THD value of (0.72%), high efficiency of (96.85%), high Tracking efficiency (98.92%) and minimized RMSE error rate is accomplished by the proposed technique.

REFERENCES

- [1] Kavin, K. S., and P. Subha Karuvelam. "PV-based grid interactive PMBLDC electric vehicle with high gain interleaved DC-DC SEPIC Converter." *IETE Journal of Research* 69, no. 7 (2023): 4791-4805.
- [2] Pal, Pikaso, and V. Mukherjee. "Off-grid solar photovoltaic/hydrogen fuel cell system for renewable energy generation: An investigation based on techno-economic feasibility assessment for the application of end-user load demand in North-East India." *Renewable and Sustainable Energy Reviews* 149 (2021): 111421.
- [3] Samy, M. M., Heba I. Elkhoully, and S. Barakat. "Multi-objective optimization of hybrid renewable energy system based on biomass and fuel cells." *International Journal of energy research* 45, no. 6 (2021): 8214-8230.
- [4] Geleta, Diriba Kajela, and Mukhdeep Singh Manshahia. "Gravitational search algorithm-based optimization of hybrid wind and solar renewable energy system." *Computational Intelligence* 38, no. 3 (2022): 1106-1132.
- [5] Mosaad, Mohamed I., Haitham Saad Mohamed Ramadan, Mansour Aljohani, Mohamed F. El-Naggar, and Sherif SM Ghoneim. "Near-optimal PI controllers of STATCOM for efficient hybrid renewable power system." *IEEE Access* 9 (2021): 34119-34130.
- [6] Dorn-Gomba, Lea, John Ramoul, John Reimers, and Ali Emadi. "Power electronic converters in electric aircraft: Current status, challenges, and emerging technologies." *IEEE Transactions on Transportation Electrification* 6, no. 4 (2020): 1648-1664.
- [7] Hasanpour, Sara, Mojtaba Forouzesh, Yam P. Siwakoti, and Frede Blaabjerg. "A new high-gain, high-efficiency SEPIC-based DC-DC converter for renewable energy applications." *IEEE Journal of Emerging and Selected Topics in Industrial Electronics* 2, no. 4 (2021): 567-578.
- [8] Khalili, Siamak, Navid Molavi, and Hosein Farzanehfard. "Soft-switched asymmetric interleaved WCCI high step-down converter with low-voltage stress." *IEEE Journal of Emerging and Selected Topics in Power Electronics* 9, no. 6 (2021): 6692-6699.
- [9] Tarzamni, Hadi, Mehran Sabahi, Saeed Rahimpour, Matti Lehtonen, and Payman Dehghanian. "Operation and design consideration of an ultrahigh step-up DC-DC converter featuring high power density." *IEEE Journal of Emerging and Selected Topics in Power Electronics* 9, no. 5 (2021): 6113-6123.
- [10] Belhaouas, N., F. Mehareb, H. Assem, E. Kouadri-Boudjelthia, S. Bensalem, F. Hadjrioua, A. Aissaoui, and K. Bakria. "A new approach of PV system structure to enhance performance of PV generator under partial shading effect." *Journal of Cleaner Production* 317 (2021): 128349.
- [11] AlZubaidi, Asaad AH, Laith Abdul Khaliq, Hassan Salman Hamad, Waleed Khalid Al-Azzawi, Mohanad Sameer Jabbar, and Thaer Abdulwahhab Shihab. "MPPT implementation and simulation using developed P&O algorithm for photovoltaic system concerning efficiency." *Bulletin of Electrical Engineering and Informatics* 11, no. 5 (2022): 2460-2470.
- [12] Ahmed, Sajib, Saad Mekhilef, Marizan Binti Mubin, and Kok Soon Tey. "Performances of the adaptive conventional maximum power point tracking algorithms for solar photovoltaic system." *Sustainable Energy Technologies and Assessments* 53 (2022): 102390.
- [13] Ali, Mahmoud N., Karar Mahmoud, Matti Lehtonen, and Mohamed MF Darwish. "An efficient fuzzy-logic based variable-step incremental conductance MPPT method for grid-connected PV systems." *Ieee Access* 9 (2021): 26420-26430.
- [14] Gunasekaran, Maheswaran, Vijayakumar Krishnasamy, Sivakumar Selvam, Dhafer J. Almakhlles, and Norma Anglani. "An adaptive resistance perturbation based MPPT algorithm for photovoltaic applications." *IEEE Access* 8 (2020): 196890-196901.
- [15] Ibrahim, Al-wesabi, M. B. Shafik, Min Ding, Mohammad Abu Sarhan, Zhijian Fang, Ahmed G. Alareqi, Tariq Almoqri, and Ayman M. Al-Rassas. "PV maximum power-point tracking using modified particle swarm optimization under partial shading conditions." *Chinese Journal of Electrical Engineering* 6, no. 4 (2020): 106-121.

- [16] Alkahtani, Ammar Ahmed, Saad TY Alfalahi, Abedalgany Abedallah Athamneh, Ali Q. Al-Shetwi, Muhamad Bin Mansor, M. A. Hannan, and Vassilios G. Agelidis. "Power quality in microgrids including supraharmonics: Issues, standards, and mitigations." *IEEE access* 8 (2020): 127104-127122.
- [17] Kumar, Gaurav, Mithilesh Singh, and Gokul Dewangan. "RELIABILITY AND POWER QUALITY IMPROVEMENT OF WIND INTEGRATED TRANSMISSION SYSTEM USING STATCOM FOR NON-LINEAR LOADS."
- [18] Zaidan, Majeed Rashid, and Saber Izadpanah Toos. "Optimal location of static var compensator to regulate voltage in power system." *IETE Journal of Research* 69, no. 4 (2023): 2177-2185.
- [19] ZAKRI, AZRIYENNI AZHARI, TAUFUQ RAHMAN SIREGAR, MOHD WAZIR MUSTAFA, and WAHRI SUNANDA. "Modelling and Analysis using The Thyristors Controlled Series Compensators for Electrical Power Systems." *ELKOMIKA: Jurnal Teknik Energi Elektrik, Teknik Telekomunikasi, & Teknik Elektronika* 11, no. 3 (2023): 691.
- [20] Savaliya, Ankit, and Sanath Alahakoon. "Mitigation of Power Quality Problems Associated with Solar PV Integration into Low Voltage Distribution Network in India." In *2020 Australasian Universities Power Engineering Conference (AUPEC)*, pp. 1-6. IEEE, 2020.
- [21] Singh, Rishi Kumar, and Nikhil Kumar Singh. "Power system transient stability improvement with FACTS controllers using SSSC-based controller." *Sustainable Energy Technologies and Assessments* 53 (2022): 102664.
- [22] Mohamed, Ahmed Abdel Rahman, Hebatallah Mohamed Sharaf, and Doaa Khalil Ibrahim. "Enhancing distance protection of long transmission lines compensated with TCSC and connected with wind power." *IEEE Access* 9 (2021): 46717-46730.
- [23] Millah, Ibrahim Saiful, Pei Cheng Chang, Dawit Fekadu Teshome, Ramadhani Kurniawan Subroto, Kuo Lung Lian, and Jia-Fu Lin. "An enhanced grey wolf optimization algorithm for photovoltaic maximum power point tracking control under partial shading conditions." *IEEE Open Journal of the Industrial Electronics Society* 3 (2022): 392-408.
- [24] Suhardi, Diding, Lailis Syafaah, Muhammad Irfan, M. Yusuf, M. Effendy, and I. Pakaya. "Improvement of maximum power point tracking (MPPT) efficiency using grey wolf optimization (GWO) algorithm in photovoltaic (PV) system." In *IOP Conference Series: Materials Science and Engineering*, vol. 674, no. 1, p. 012038. IOP Publishing, 2019.
- [25] Yan, Chang, Guoping Lei, Li Cai, Chao He, Nina Dai, Zhou Jiang, Jiacheng Wu, and Shenghao Li. "MPPT control technology based on the GWO-VINC algorithm." *Frontiers in Energy Research* 11 (2023): 1205851.